Pharm Res (2011) 28:2745–2757
DOI 10.1007/s11095-011-0492-8

EXPERT REVIEW

Quantitative Glucose and ATP Sensing in Mammalian Cells

Dania C. Liemburg-Apers • Hiromi Imamura • Marleen Forkink • Marco Nooteboom • Herman G. Swarts • Roland Brock • Jan A. M. Smeitink • Peter H. G. M. Willems • Werner J. H. Koopman

Received: 17 February 2011 / Accepted: 24 May 2011 / Published online: 21 June 2011

ABSTRACT The functioning and survival of mammalian cells requires an active energy metabolism. Metabolic dysfunction plays an important role in many human diseases, including diabetes, cancer, inherited mitochondrial disorders, and metabolic syndrome. The monosaccharide glucose constitutes a key source of cellular energy. Following its import across the plasma membrane, glucose is converted into pyruvate by the glycolysis pathway. Pyruvate oxidation supplies substrates for the ATP-generating mitochondrial oxidative phosphorylation (OXPHOS) system. To gain cell-biochemical knowledge about the operation and regulation of the cellular energy metabolism in the healthy and diseased state, quantitative knowledge is required about (changes in) metabolite concentrations under (non) steady-state conditions. This information can, for instance, be used to construct more realistic *in silico* models of cell metabolism, which facilitates understanding the consequences of metabolic dysfunction as well as on- and off-target effects of mitochondrial drugs. Here we review the current state-of-the-art live-cell quantification of two key cellular metabolites, glucose and ATP, using protein-based sensors. The latter apply the principle of FRET (fluorescence resonance energy transfer) and allow measurements in different cell compartments by fluorescence microscopy. We further summarize the properties and applications of the FRET-based sensors, their calibration, pitfalls, and future perspectives.

KEY WORDS ATeam · fibroblast · GLUT · systems biology

ABBREVIATIONS

2-DG	2-Deoxy-D-glucose
A	fluorescence acceptor molecule
AcCoA	acetyl-coenzyme A
ADP	adenoside diphosphate
AMP	adenosine monophosphate
AMPK	AMP-activated protein kinase
ANT	adenine nucleotide translocator
ATP	adenoside triphosphate
D	fluorescence donor molecule
DNP	2,4-Dinitrophenol
ECFP	enhanced cyan fluorescent protein
ER	endoplasmic reticulum
EYFP	enhanced yellow fluorescent protein
FCCP	carbonyl cyanide-p-trifluoromethoxyphenylhydrazone
FRET	fluorescence resonance energy transfer
FS	fractional saturation
G6P	glucose-6-phosphate
GFP	green fluorescent protein
GGBP	glucose galactose-binding protein
GK	glucokinase
GLUT	glucose transporter

D. C. Liemburg-Apers • M. Forkink • M. Nooteboom • H. G. Swarts • R. Brock • P. H. G. M. Willems • W. J. H. Koopman (✉)
Department of Biochemistry (286)
Nijmegen Centre for Molecular Life Sciences
Radboud University Nijmegen Medical Centre
P.O. Box 9101
NL-6500 HB, Nijmegen, The Netherlands
e-mail: w.koopman@ncmls.ru.nl

D. C. Liemburg-Apers • M. Nooteboom • J. A. M. Smeitink
Department of Pediatrics
Nijmegen Centre for Mitochondrial Disorders
Radboud University Nijmegen Medical Centre
Nijmegen, The Netherlands

D. C. Liemburg-Apers • M. Nooteboom • J. A. M. Smeitink • P. H. G. M. Willems • W. J. H. Koopman
Centre for Systems Biology and Bioenergetics
Radboud University Nijmegen Medical Centre
Nijmegen, The Netherlands

H. Imamura
Kyoto University
Kyoto, Japan

HK	hexokinase
IAA	iodoacetate
LDH	lactate dehydrogenase
OFP	orange fluorescent protein
OXPHOS	oxidative phosphorylation
PBP	periplasmic binding protein
PDH	pyruvate dehydrogenase
PFK	phosphofructokinase
PK	pyruvate kinase
PKC	protein kinase C
PM	plasma membrane
PPP	pentose phosphate pathway
ROS	reactive oxygen species
SGLT	sodium-dependent glucose cotransporters
SLO	*streptolysin O*
SNR	signal-to-noise ratio
TCA	tricarboxylic acid
TPA	phorbol 12-myristate 13-acetate
VDAC	voltage-dependent anion channel

INTRODUCTION

Energy availability in a living cell depends on the balance between energy production by breakdown of biomolecules (catabolism) and energy demand. This balance constitutes part of a cell's metabolism, which involves a large collection of molecular intermediates (metabolites). The concentration of metabolites continually changes in time and/or space in response to alterations in the cellular environment and metabolic activity. Within cells, adenosine triphosphate (ATP) is the most important energy currency. ATP hydrolysis yields adenosine diphosphate (ADP) and inorganic phosphate (P_i), providing the energy that fuels numerous cellular processes. In most cells, ATP is generated by the metabolic conversion of the monosaccharide glucose, which is taken up from the extracellular environment. In this sense, glucose and ATP are key players in cellular metabolism. Directly below we provide a brief introduction into cellular glucose and ATP metabolism. Next, we present how protein-based sensors can be used to quantify the (sub)cellular concentration of glucose and ATP. Finally, we discuss sensor calibration, possible pitfalls and future perspectives.

CELLULAR GLUCOSE AND ATP METABOLISM

Glucose is a monosacharide ($C_6H_{12}O_6$), present in most dietary carbohydrates, that is ubiquitously used as a source of cellular energy. Cellular uptake of glucose can take place via active and passive mechanisms. Active glucose uptake, for instance, occurs in the enterocytes of the intestine and the epithelial cells of the proximal tubuli of the nephrons in the kidney. This uptake is performed by sodium-dependent glucose cotransporters (SGLTs). However, in the majority of mammalian cells, glucose is taken up from the extracellular environment (*e.g.* the blood) through facilitated diffusion mediated by glucose transporters (GLUTs). In the cytosol, glucose is phosphorylated and converted into pyruvate by glycolysis (Fig. 1). Pyruvate can be taken up by mitochondria, where it is used to generate reduced nicotinamide adenine dinucleotide (NADH) and reduced flavin adenine dinucleotide ($FADH_2$). The latter serve as substrates for the oxidative phosphorylation (OXPHOS) system to maintain ATP homeostasis and fuel energy-consuming cellular processes (Fig. 1).

GLUT Properties and Regulation

GLUTs are integral membrane proteins that belong to the Major Facilitator Superfamily (MFS) of membrane transporters (1) and contain twelve membrane spanning helices. Both the N- and C-terminus of the protein are located on the cytoplasmic side of the plasma membrane (PM). The transport capacity of a specific GLUT at a given time can be controlled by several regulatory mechanisms in an isoform and cell type-specific manner. In humans, fourteen members of the GLUT family have been identified which differ in their tissue distribution, kinetic properties, substrate specificity, intracellular localization, and mode of regulation (1).

GLUT1 is the most common isoform and is highly expressed in astrocytes, erythrocytes, and endothelial cells (*e.g.* (2,3)). GLUT1 has a K_m (being the substrate concentration at which the enzyme functions at half of its maximal capacity; V_{max}) for glucose between 1–2 mM and mediates basal glucose uptake. In several cell types, GLUT1 expression increases upon deprivation of glucose, leading to an increased overall glucose transport capacity of the cell. *Vice-versa*, GLUT1 expression is decreased in the presence of high levels of glucose, leading to a decreased overall glucose transport capacity (*e.g.* (4)). In addition, GLUT1 expression is often increased in many tumor cells (5), compatible with their glycolytic mode of ATP generation (6). In mature erythrocytes, which exclusively rely on glycolysis for ATP production, high levels of ATP induce an acute decrease in the intrinsic transport capacity of GLUT1 (3). This effect is explained by ATP interacting with the cytoplasmic loop between transmembrane segments 8 and 9 of GLUT1, which induces a global conformational change in the cytoplasmic loops 6 and 7 and the C-terminal domain, resulting in their interaction and a limited glucose influx into the cytosol. Conversely, ATP depletion enhances the intrinsic transport capacity of GLUT1. Adenosine monophosphate (AMP) functions as a competitive antagonist for ATP-dependent inhibition of GLUT1 transport capacity. This

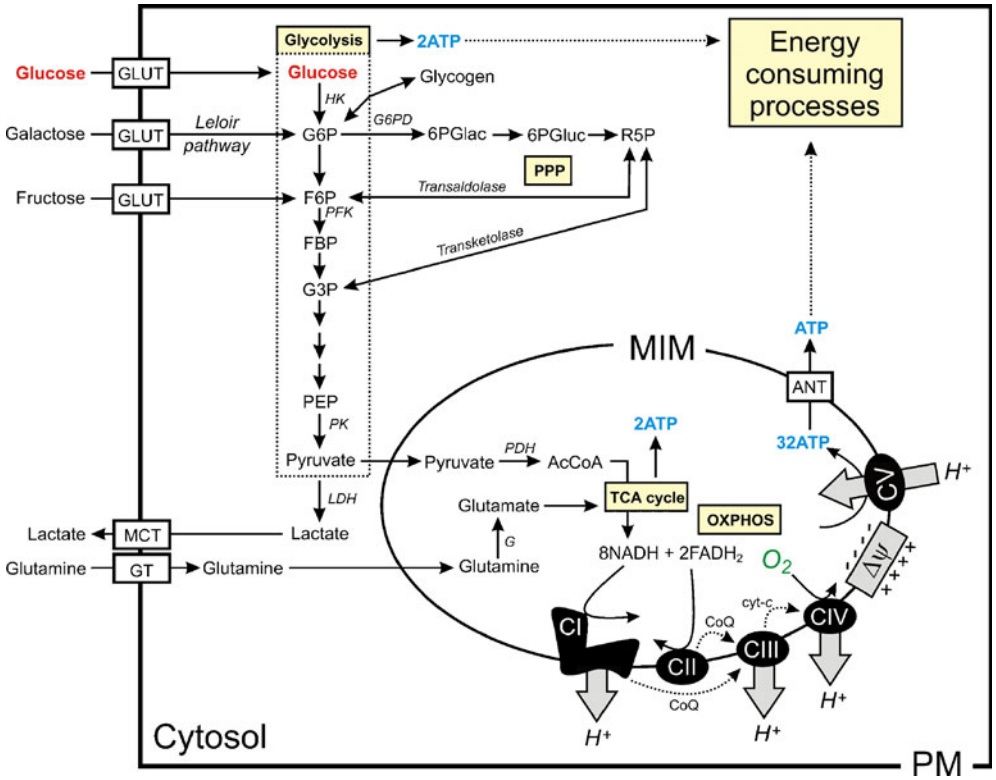

Fig. 1 Key cellular metabolic pathways. Glucose enters the cell via glucose transporters (GLUT) and is subsequently converted into ATP, NADH, and pyruvate by glycolysis. Alternatively, surplus glucose can be stored in the cell as glycogen. Within the mitochondrion, pyruvate is converted into acetyl-coenzyme-A (AcCoA). The latter is used by the tricarboxylic acid (TCA) cycle to generate ATP, NADH and $FADH_2$. Subsequently, mitochondrial oxidative phosphorylation (OXPHOS) converts NADH and $FADH_2$ into ATP, which is exported to the cytosol by the adenine nucleotide translocator (ANT) to fuel energy-consuming processes. OXPHOS-mediated (aerobic) ATP production requires molecular oxygen (O_2). As a net result of the above pathway, 36 molecules of ATP can be generated for each glucose molecule consumed (2 ATP by glycolysis, 2 ATP by the TCA cycle and 32 ATP by OXPHOS). Glucose metabolites can be redirected into the pentose phosphate pathway (PPP). Also galactose (via the Leloir pathway), fructose and glutamine can be used as energy sources. Figure adapted from (6). Δψ, mitochondrial membrane potential; 6PGlac, 6-P-gluconolactone; 6PGluc, 6-P-gluconate; ANT, adenine nucleotide translocator; CI-CV, complex I-V; CoQ, coenzyme Q_{10}; Cyt-*c*, cytochrome *c*; $FADH_2$, reduced flavin adenine dinucleotide; FBP, fructose-1,6-biphosphate; F6P, fructose-6-phospate; G, Glutaminase; G3P, glyceraldehyde-3-phosphate; G6P, glucose-6-phosphate; G6PD, Glucose-6-phosphate dehydrogenase; GT, Glutamine transporter; HK, Hexokinase; LDH, Lactate dehydrogenase; MCT, Monocarboxylate transporter; MIM, mitochondrial inner membrane; NADH, reduced nicotinamide adenine dinucleotide; PDH, Pyruvate-dehydrogenase; PEP, phosphoenol-pyruvate; PFK, Phospho-fructo-kinase; PK, Pyruvate kinase; PM, plasma membrane; PPP, Pentose phosphate pathway; R5P, ribose-5-phosphate.

suggests that in cells where GLUT1 is the predominant glucose transporter, glucose transport depends on substrate availability and cellular metabolic state.

GLUT2 is highly expressed in the liver, enterocytes of the intestine, epithelial cells of the kidney, hepatocytes, and β-cells of the pancreas, which play important roles in whole body glucose homeostasis. GLUT2 is a transporter with a K_m for glucose of 15–20 mM (*i.e.* a lower affinity than GLUT1) and a high capacity for glucose transport. This allows for increased glucose uptake at high concentrations. Although most GLUT transporters have the potential to transport glucose both in and out of the cell, glucose export can only occur when the intracellular glucose concentration exceeds the extracellular glucose concentration. In the above-mentioned tissues, intracellular glucose concentrations can be high, and glucose export is mediated by GLUT2. For example, in the enterocytes of the intestine, glucose is actively taken up by SGLT1 at the apical membrane of the enterocytes, which increases the intracellular glucose concentration. When the intracellular glucose concentration exceeds the glucose concentration in the blood, glucose is released from the enterocytes into the bloodstream by GLUT2 at the basolateral membrane. Only when glucose concentrations in the intestinal lumen exceed the transport capacity of the SGLT1s, GLUT2 can translocate to the apical membrane of the enterocytes to increase the cells transport capacity for glucose (7). In a reaction to increasing blood glucose levels, insulin mediates GLUT2 internalization from the apical and basolateral membrane (8). GLUT2 also mediates glucose uptake in the liver, where it is stored as glycogen, when the glucose concentration in the blood is high (Fig. 1). When glucose levels in the blood are low, glucose-6-phosphate (G6P) is produced from glycogen and dephosphorylated in the

lumen of the endoplasmic reticulum (ER). Subsequently, glucose can be either transported to the cytosol before release into the blood by GLUT2 or exported by vesicular transport (9). In hepatocytes, transcription of GLUT2 is stimulated by active glucose metabolism (10).

GLUT3 is expressed in cells with a high energy demand, including neurons. GLUT3 has a relatively high affinity (K_m = 1 mM) and transport capacity for glucose and is suggested to enable neurons to have preferential access to the available glucose in the brain (11).

GLUT4 is expressed in insulin-responsive tissues such as skeletal and cardiac muscle and adipocytes and has a K_m of 5 mM. In these cells, insulin stimulates glucose transport capacity by increasing GLUT4 incorporation in the PM. Insulin binding to the insulin receptor leads to stimulation of exocytosis of GLUT4-containing vesicles. When insulin levels in the blood decrease, GLUT4 is internalized from the PM. ATP-dependent regulation of glucose transport capacity as described above for GLUT1 has also been suggested for GLUT4 (12).

Glycolysis

In the cytosol, the enzymes of the glycolysis pathway carry out the oxidation of glucose to pyruvate in a step-wise manner. This process generates 2 ATP molecules for each glucose molecule that is consumed. Alternative glycolysis substrates include galactose and fructose, which enter the glycolytic pathway as glucose-6-phosphate (G6P) and fructose-6-phosphate (F6P), respectively (Fig. 1). The first step in glucose metabolism is its phosphorylation by hexokinase (HK), generating glucose-6-phosphate (G6P), which cannot be exported from the cell (Fig. 1). G6P can be converted into glycogen (energy storage), further metabolized via glycolysis (pyruvate production), or enter the anabolic pentose phosphate pathway (PPP), which plays a role in nucleotide biosynthesis and detoxification. The rate of glycolysis is cell type-dependent due to the tissue-specific isoform distribution of glycolytic enzymes, cell cycle phase, and cell differentiation. Moreover, the glycolytic rate can be altered by cell stimuli, substrate availability, aging, and disease conditions. Regulation of the glycolytic rate occurs at the level of the glycolytic enzymes HK, phosphofructokinase (PFK), and pyruvate kinase (PK). Three HK isoforms (HKI-III) are allosterically auto-inhibited by G6P. Furthermore, HKI and II can interact with mitochondria by forming a complex with the voltage-dependent anion channel (VDAC) and adenine nucleotide translocator (ANT) on the mitochondrial outer membrane (MOM). This allows direct utilization of mitochondria-generated ATP, exported from the mitochondrion by the ANT, for glucose phosphorylation (13). The amount of mitochondria-bound HKs is cell type-dependent and often increased in tumor cells. Interestingly, HKs attached to mitochondria are less sensitive to G6P auto-inhibition. Glucokinase (GK) also catalyzes the formation of G6P from glucose and is expressed in the liver, the pancreas, the small intestine, and the brain. GK has an approximately 100 times lower glucose affinity (K_m = 8 mM) than HKs (K_m = 70 μM) and is not inhibited by G6P. In normal differentiated cells the absence of sufficient molecular oxygen (O_2) required for mitochondrial oxidative phosphorylation (see next section) stimulates the conversion of pyruvate into lactate by lactate dehydrogenase (LDH). The lactate formed is then exported out of the cell. However, most cancer cells rely mainly on glycolysis for ATP generation, even in the presence of O_2. This phenomenon is called the 'Warburg effect' (6).

OXPHOS

Glycolysis-derived pyruvate is imported into mitochondria and converted into acetyl-coenzyme-A (AcCoA) by pyruvate dehydrogenase (PDH). AcCoA is further oxidized by enzymes of the tricarboxylic acid (TCA) cycle to generate 2 ATP, 8 NADH and 2 $FADH_2$ molecules per glucose molecule consumed (Fig. 1). The amino acid glutamine can serve as an alternative substrate for the TCA cycle following its conversion into glutamate and α-ketoglutarate (a TCA cycle intermediate) in the mitochondrion. Alternatively, glutamate can be directly converted by glutathione cysteine ligase into reduced glutathione (GSH), a tripeptide that constitutes one of the most abundant cellular antioxidants (14).

The energy stored in NADH and $FADH_2$ is harvested by the mitochondrial OXPHOS system to generate ATP (15). Under optimal conditions, this system can yield 32 ATP molecules for each glucose molecule that is consumed. Together with the 4 ATP molecules produced by glycolysis and the TCA cycle, this in theory can give a maximum net ATP production of 36 molecules per glucose molecule consumed. The OXPHOS system is embedded in the mitochondrial inner membrane (MIM) and consists of five multi-protein complexes (complex I-V): the electron transport chain (ETC, complex I-IV) and the F_oF_1-ATP synthase (complex V). The ETC extracts electrons from NADH (at complex I) and $FADH_2$ (at complex II), which are conveyed to complex III and complex IV by MIM-associated coenzyme Q_{10} (CoQ) and cytochrome *c*, respectively. At complex IV, the electrons are donated to O_2, leading to the formation of water. The energy released during electron transport is used to expel protons from the mitochondrial matrix across the MIM. This establishes an inward-directed trans-MIM proton-motive force (PMF), which consists of a chemical (ΔpH) and electrical component ($\Delta\psi$). The energy released by the PMF-driven backflow of protons into the mitochondrial matrix is utilized by complex V to drive ATP production from

ADP and P_i. Subsequently, ATP is exported from the mitochondria via the ANT, after which it can be used to fuel energy-consuming processes.

ATP Homeostasis

Given the fact that ATP hydrolysis into ADP and P_i is reversible, *de novo* synthesis of nucleotides is generally not of major importance for intracellular ATP homeostasis in healthy cells. ADP can be formed from adenosine-monophosphate (AMP) by adenylate kinases (AKs), which catalyze the phosphorylation of AMP by ATP to yield two molecules of ADP. AMP and ATP regulate the activities of various enzymes to control ATP homeostasis. For example, AMP stimulates glucose uptake and glycolysis (via acting on GLUT1 and PFK), whereas ATP inhibits glucose uptake and glycolysis (via GLUT1, PFK and PK inhibition) and the TCA cycle (by inhibiting citrate synthase). These control mechanisms allow cells to rapidly respond to changes in intracellular ATP demand. Moreover, in muscle cells, the cellular ATP/AMP ratio modulates the rate of glycogen degradation by allosterically inhibiting glycogen phosphorylase b. Alterations in cellular energy state, reflected by changes in ATP/AMP ratio, are monitored by the AMP-activated protein kinase (AMPK). AMPK is activated by phosphorylation of the Thr172 residue within its catalytic α-subunit. Binding of AMP to the regulatory γ-subunit enhances this phosphorylation, whereas binding of ATP inhibits the phosphorylation. Therefore, AMPK becomes activated when the intracellular ATP/AMP ratio decreases. By phosphorylating a variety of downstream effector proteins, AMPK activation stimulates ATP-generating pathways (*e.g.* fatty acid oxidation) and mitochondrial biogenesis. In addition, AMPK activation inhibits ATP-consuming processes like fatty acid synthesis (16). Furthermore, AMPK regulates tight junction formation, cell polarity, cell migration, and cell death. This suggests that alterations in ATP/AMP ratio could also control these processes. The activity of several mitochondrial dehydrogenases (*e.g.* glycerol phosphate dehydrogenase, pyruvate dehydrogenase, isocitrate dehydrogenase, and β-ketoglutarate dehydrogenase) is stimulated by ionic calcium (Ca^{2+}; 17). This allows proper fueling of ATP-consuming processes like muscle contraction, membrane transport, and exocytosis, which are also activated by Ca^{2+}, and maintenance of local and global cellular ATP levels.

QUANTIFICATION OF GLUCOSE AND ATP LEVELS IN LIVING CELLS

ATP generation from glucose depends on the coupling between compartmentalized cytosolic and mitochondrial reactions. Therefore, approaches are required that allow quantification of glucose and/or ATP in the cytosol and mitochondria in single living cells. For this purpose, a variety of protein-based metabolite sensors were developed. Sensors that are based on the same principle are available for maltose, ribose and glutamate (*e.g.* (2,9,18–25)). The detection principle of most of these reporter molecules is based on the principle of Fluorescence Resonance Energy Transfer (FRET). FRET is the distance- and orientation-dependent (non-radiative) transfer of energy, which can occur between a fluorescent donor molecule (D) and a fluorescent acceptor molecule (A). FRET (D→A) only takes place if D and A are very close to each other (*i.e.* within 1–10 nm). For FRET to occur, the emission spectrum of D needs to partially overlap with the absorption spectrum of A. FRET efficiency (E) is given by $E = R_0^6/(R_0^6 + r^6)$, with r being the distance between D and A, and R_0 (the Förster distance) being the distance of half-maximal FRET efficiency. If the wavelength is expressed in cm and J(λ) is in units of $M^{-1}\cdot cm^3$, the Förster distance (in Å) for a FRET (D→A) pair is given by $R_0 = 9.78\cdot 10^3\cdot[\kappa^2\cdot n^{-4}\cdot Q_D\cdot J(\lambda)]^{1/6}$ (26). In this equation, κ^2 is a factor describing the relative orientation in space of the transition dipoles of the (D→A) pair (typically assumed to be 2/3), n is the refractive index, Q_D is the quantum-yield of D (*i.e.* the ratio of the number of photons emitted to the number absorbed), and J(λ) represents the overlap-integral, which accounts for the degree of overlap between the emission and absorption spectra of D and A, respectively.

A 'good' FRET (D→A) pair contains a D with a high quantum-yield, contains an A with a large molecular extinction coefficient, displays maximal overlap between the D emission and A absorption spectrum, and displays minimal excitation of A at the maximal excitation wavelength of D. In many biosensors, (variants of) enhanced cyan fluorescent protein (ECFP) and yellow fluorescent protein (EYFP) are used as (D→A) FRET pairs. The ECFP-EYFP pair has an R_0 of ~5.5 nm. By fusing ECFP and EYFP to the N and C termini (or *vice versa*) of a suited metabolite-sensing protein, metabolite-induced conformational changes in the sensing protein will induce changes in the ECFP→EYFP FRET signal. In this sense, metabolite binding and unbinding are associated with opposite changes in FRET efficiency that can be visualized as changes in ECFP and EYFP emission intensity by fluorescence microscopy. For instance, in the case of a sensor in which metabolite binding increases FRET efficiency, increased FRET is associated with a lower ECFP and higher EYFP fluorescence intensity, and decreased FRET is associated with higher ECFP and lower EYFP fluorescence intensity. By taking the ratio between the EYFP and ECFP emission signals, a quantitative measure of FRET is obtained.

When using FRET-based biosensors for single cell imaging, it is critical to obtain a signal with a high signal-to-noise ratio (SNR). This means that the D and A fluorescence signals need to be well above aspecific (background) fluorescence levels, which can arise from cellular autofluorescence, to prevent that small FRET changes are obscured by background noise. Additionally, the biosensor has to display large FRET changes upon concentration changes of the to-be-detected biomolecule. This means that maximizing the dynamic range of the FRET sensor is of crucial importance. To achieve the latter, one strategy is the use of 'improved' versions of CFP (*e.g.*, Cerulean, super-enhanced CFP) and YFP (*e.g.*, Venus, Citrine) because the FRET efficiency generally depends on the photo-physical properties of the D and A fluorophores. Another way to improve the dynamic range is to replace the normal FPs in the FRET sensor by circularly permuted fluorescent proteins (cpFPs), in which the native N- and C-termini are connected by a linker, and new termini are created in a loop region (27). In a FRET biosensor with such proteins, the relative orientation of the two fluorophores will differ from that in non-circularly permuted fluorescent proteins.

FRET-Based Biosensors for Glucose Sensing

Bacterial periplasmic binding proteins (PBPs) have been applied as sensing proteins in FRET-based biosensors. PBPs display a high affinity for specific metabolites and possess considerable similarity at the level of their tertiary structure. PBPs consist of two globular domains that are connected by a hinge region. Substrate binding occurs in the cleft between the globular domains, and the substrate is engulfed via a hinge-twist motion, leading to a major conformational change in the protein. By flanking the PBP with a donor and acceptor fluorescent protein, the conformational change occurring in the PBP is translated into a change in FRET. The PBP family can be divided into two classes. In type I PBPs, the N- and C-terminus are located at the proximal ends of the globular domains. Upon substrate binding, the termini and fluorophores in the sensor move further apart from each other, and FRET is decreased (18). In type II PBPs, the termini are located at the distal ends of the globular domains and move closer to each other upon substrate binding, leading to an increase in FRET. The majority of the FRET-based glucose biosensors use the periplasmic glucose/galactose-binding protein (GGBP) from the bacterium *E. coli* for glucose sensing. GGBP is a type I PBP and is involved in chemotaxis towards glucose and galactose in many bacteria, so GGBP is able to detect both glucose and galactose, but its affinity for glucose is approximately two times higher compared to galactose (18). Although the precise galactose concentration in cells is not firmly established, the plasma galactose concentration in healthy humans (0.17 mM) is far below that of blood glucose (5 mM). GGBP-based glucose sensors do not directly respond to the glycolysis-inhibitor 2-Deoxy-D-glucose (2-DG) (18).

One of the first FRET-based glucose sensors consisted of a GGBP flanked by ECFP and EYFP and was designated "fluorescence indicator protein for glucose with an *in vitro* K_d of 170 nM" ("FLIPglu-170n"; Table 1). This sensor contains the wild-type GGBP, displaying a relatively high affinity for glucose. However, the blood glucose concentration is much higher (see previous section), and, therefore, intracellular glucose levels might be far above the K_d of FLIPglu-170n.

To allow quantification of higher glucose levels, Phe16 in GGBP was mutated into an alanine. This reduced the substrate affinity of GGBP, resulting in a sensor with a K_d of 590 μM, (FLIPglu-600μ; Table 1). Relative to FLIPglu-170n, FLIPglu-600μ also displayed a somewhat higher maximum EYFP/ECFP ratio change and increased glucose specificity. A "control" sensor was generated by mutating aspartic acid at position 236 in GGBP to an alanine, leading to greatly decreased glucose sensitivity ("FLIPglu-control"; $K_d \geq 100$ mM; Table 1).

To further increase the maximum ratio change of FLIPglu-600μ, two strategies were applied to reduce the rotational freedom of its two fluorophores (20). In a first approach, the sensor-structure was made more rigid by deleting various amino acids of the 'composite linkers', being the less well-structured sequences connecting the fluorophores to the GGBP. The mutant with a deletion of 15 amino acids in the N-terminal linker and 16 amino acids in the C-terminal linker, named FLIPglu-600μΔ13, showed the highest increase in maximum ratio change relative to FLIPglu-600μ (Table 1). The second approach involved the insertion of ECFP into the backbone of GGBP to decrease its rotational freedom. Additionally, EYFP was replaced by Citrine, a YFP mutant which is less pH- and chloride-sensitive than EYFP and displays an increased *in vivo* folding efficiency (28). The resulting sensor, "fluorescent indicator—ECFP insertion at position 12—protein for glucose with an *in vitro* K_d of 590 μM" (FLII^{12}Pglu-600μ) displayed the highest increase in maximum ratio change compared to FLIPglu-600μ (Table 1).

In an attempt to increase the maximum ratio change even further, various amino acid deletions were created in the composite linker between GGBP and Citrine of FLII^{12}Pglu-600μ (29). The mutant in which only the six amino acids of the synthetic linker between GGBP and Citrine were removed (FLII^{12}Pglu-700μδ6) displayed the highest *in vivo* ratio change relative to FLII^{12}Pglu-600μ (Table 1). Furthermore, by mutating the GGBP, a range of affinity mutants was engineered (*i.e.* FLIPglu-170nΔ13, FLIPglu-2μΔ13, FLIPglu-3.2mΔ13, FLIPglu-30μΔ13) to

Table 1 Properties of FRET-Based Glucose and ATP Biosensors

Sensor name	K_d (μM)[a]	Range (μM)[b]	Ratio change[c]	FRET pair[d]	Reference
GLUCOSE SENSORS					
FLIPglu-170n	0.17	0.02–1.5	−0.23	ECFP→EYFP	(18)
FLIPglu-600μ	590	65–5301	−0.29	ECFP→EYFP	(18)
FLIPglu-600$\mu\Delta$13	590	n.r.	−0.7	ECFP→EYFP	(20)
FLII^{12}Pglu-600μ	583	n.r.	2.66	ECFP→Citrine	(20)
FLIPglu-3.2mΔ13	3200	n.r.	−0.6	ECFP→EYFP	(22)
FLIPglu-2$\mu\Delta$13	2	n.r.	−0.8	ECFP→EYFP	(22)
FLIPglu-170nΔ13	0.17	n.r.	−0.8	ECFP→EYFP	(22)
FLII^{12}Pglu-700$\mu\delta$6	660	50–9600	2.3	ECFP→Citrine	(29)
FLIPglu-30$\mu\Delta$13	28.5	n.r.	n.r.	ECFP→Venus	(31)
FLIPglu-control (CT)	>100,000	n.a.	n.a.	ECFP→EYFP	(18)
ATP SENSORS					
AT1.03	3300	800–7000	1.39[e]	mseCFP(ΔC11)→cp173-mVenus	(25)
AT1.03^{YEMK}	1200	300–4000	1.83[e]	mseCFP(ΔC11)→cp173-mVenus	(25)
AT3.10^{MGK}	14	4–60	0.97[f]	mseCFP(ΔC10)→mVenus	(25)
AT3.10	7.4	2–30	1.66[f]	mseCFP(ΔC10)→mVenus	(25)
AT1.03(nD/nA)	2400	500–5000	1.98[e]	seCFP(ΔC11)→cp173-Venus	(37)
AT1.03$^{R122K/R126K}$ (CT)	>10,000	n.a.	n.a.	mseCFP(ΔC11)→cp173-mVenus	(25)
GO-ATeam1	7100	2000–20000	0.34[g]	cp173-mEGFP→mKOκ	(38)
GO-ATeam2	2300	500–5000	0.60[h]	cp173-mEGFP→mKOκ	(38)

[a] Determined *in vitro*

[b] Dynamic detection range

[c] Maximal ratio change determined *in vitro*. This value might vary with experimental conditions. Positive values indicate that FRET efficiency is increased upon glucose or ATP binding. Negative values indicate that FRET efficiency is decreased upon glucose binding.

[d] Donor→Acceptor FRET pair

[e] Determined from difference between ratios at 0 and 10 mM MgATP

[f] Determined from difference between ratios at 0 and 100 μM MgATP

[g] Determined from difference between ratios at 0 and 30 mM MgATP

[h] Determined from difference between ratios at 0 and 18 mM MgATP

CT control; *ECFP* enhanced cyan fluorescent protein; *EYFP* enhanced yellow fluorescent protein; *FRET* fluorescence resonance energy transfer; *mKO*κ monomeric Kusabira Orange κ; *msecCFP* monomeric super-enhanced cyan fluorescent protein; *n.a.* not appropriate, *n.r.* not reported in the cited reference

cover a wide range of glucose affinities (Table 1). In the case of FLIPglu-30$\mu\Delta$13, EYFP was replaced by a mutant variant (Venus), which displays improved *in vivo* maturation (30).

Application of FRET-Based Glucose Sensors

The glucose sensors introduced above have been applied in a collection of mammalian cell lines to assess steady-state glucose levels and flux rates under a variety of experimental conditions. For instance, FLIPglu-600μ was used to analyze glucose dynamics in the cytosol of COS-7 cells (18). It was found that this sensor responded rapidly to changes in extracellular glucose concentration in a reversible manner. Using the *in vitro* K_d of FLIPglu-600μ, the cytosolic glucose concentration in COS-7 was estimated to be generally 50% lower than the extracellular glucose concentration. This suggests that glucose is metabolized at a high rate in these cells. In C2C12 muscle cells, the FLIPglu-600μ sensor revealed a higher glucose concentration near the PM and a lower perinuclear concentration (5). The latter might be due to the presence of hexokinases bound to perinuclear mitochondria. When C2C12 cells were cultured in a medium with a high-glucose concentration (25 mM), cytosolic glucose levels were lower than when cells were cultured in a low-glucose medium (<5 mM). High external glucose levels reduced the rate of glucose uptake in Chinese hamster ovary (CHO) cells, suggesting down-regulation of GLUT1. In these cells, the cytosolic glucose concentration was maintained at ~1 mM when extracellular glucose concentration equaled 10 mM (5). In CHO cells displaying a low glucose uptake rate, cytosolic glucose accumulation

was observed upon glycolysis inhibition by iodoacetate (IAA). Glucose uptake was not affected by glycolysis inhibition. Upon removal of extracellular glucose there was little glucose clearance, suggesting that glucose efflux is absent. In contrast, in cells displaying a high glucose uptake rate, less glucose accumulation was observed upon inhibition of glycolysis (5). When human embryonic kidney (HEK) cells were cultured in a high-glucose medium, the rate of decrease in cytosolic glucose concentration was increased in response to acute changes in extracellular glucose concentration, suggesting that glycolytic enzymes are more active in these cells (5). When cells were pre-cultured in a high-glucose medium, acute lowering of the extracellular glucose concentration increased cytosolic glucose levels, possibly by stimulating the generation of glucose from non-carbohydrate carbon substrates (*i.e.* gluconeogenesis) (5). Conversely, cells pre-cultured in a low-glucose medium displayed a decrease in intracellular glucose level upon acutely increasing the extracellular glucose level, suggesting that glycolysis is stimulated by low external glucose. Taken together, the above findings suggest a mechanism in which glucose homeostasis is dynamically controlled by alterations in glucose transport and metabolism. This mechanism might serve to prevent toxic effects of too high cytosolic glucose as well as to prevent the glucose level from dropping below the K_m of HK.

FLIPglu-600μ was also applied to measure glucose fluxes between the ER and cytosol (9). To this end, FLIPglu-600μ was modified to contain ER targeting and retention signals. No differences between the cytosolic and ER glucose concentration were observed. Similarly, the glucose flux rate across the ER membrane and PM did not differ. However, when a high-affinity glucose sensor was used (FLIPglu-30μΔ13) and measurements were carried out in low-glucose medium, the steady-state glucose concentration, as well as the glucose flux rate across the ER membrane and PM, were different (31). The latter study also revealed that, following their biosynthesis in the ER, GLUTs were active during their transport to the PM and mediated glucose transport over the ER membrane.

Using FLI^{12}Pglu-700μδ6, the glycolytic rate was investigated in fibroblasts, adipocytes, myoblasts, astrocytes, neurons, and HeLa cells (2). To this end, glucose transport across the PM was reduced either by lowering the extracellular glucose concentration or by specifically inhibiting GLUTs. Average glycolytic rates were demonstrated to be higher in undifferentiated cells (C2C12 myoblasts and 3T3-L1 fibroblasts) and tumor cell lines (HeLa cells) than in astrocytes, neurons, and differentiated 3T3-L1 adipocytes. Moreover, the variability in glycolytic rate between individual cells was higher for astrocytes, 3T3-L1 fibroblasts, C2C12 myoblasts, and HeLa cells, when compared to neurons and 3T3-L1 adipocytes.

FRET-Based Biosensors for ATP Sensing

The first ATP biosensor was originally developed to detect conformational changes in the ATP-sensitive potassium (K_{ATP}) channel Kir6.2 (19). In this reporter molecule, Kir6.2 is flanked by ECFP and EYFP (ECFP-Kir6.2-EYFP), and ATP binding induces a conformational change in Kir6.2, thereby altering FRET efficiency. However, the pH dependence of this change and its specificity for ATP is unclear. Moreover, the FRET dynamic range of ECFP-Kir6.2-EYFP is quite small, suggesting that it may not be an optimal ATP biosensor. Recently, two new types of fluorescent ATP biosensors were introduced. One is the "Perceval" biosensor, which is sensitive to the ATP/ADP ratio (24), while the other is the "ATeam" biosensor ("Adenosine 5′-Triphosphate indicator based on Epsilon subunit for Analytical Measurements"), which is sensitive to ATP concentration (25).

Perceval consists of a circularly permuted (32) monomeric Venus (cpmVenus) inserted into GlnK1, a bacterial protein that regulates ammonia transport (24). ATP and ADP bind competitively to GlnK1 (K_d=0.04 μM for ATP, 0.2 μM for ADP). Nucleotide binding induces a conformational change in GlnK1, which alters the conformation of Venus. As a consequence, the Venus fluorescence excitation spectrum changes: the major excitation peak at 490 nm is enhanced, while the minor excitation peak at 405 nm is reduced. Since ATP-binding induces a larger conformational change than ADP-binding, ATP induces a larger change in fluorescence than ADP. However, the pH sensitivity of Perceval makes its fluorescence signal difficult to interpret.

ATeam (AT1.03) is a FRET-based biosensor consisting of the regulatory ε subunit of the F_oF_1-ATP synthase complex from *Bacillus subtilis* flanked by CFP and YFP. There are two domains in the ε subunit, namely, the N-terminal β-sandwich domain and the C-terminal α-helical domain. ATP binds to the interface between the two domains with a K_d-value of 3.3 mM and induces a large conformational change in the C-terminal domain from an open to a closed configuration (33). This conformational change alters the distance and orientation between the two fluorescent proteins, resulting in an increased FRET efficiency. AT1.03 fluorescence is not affected by the presence of other nucleotides (*i.e.* ADP, dATP and GTP; 0-10 mM) and by changes in pH above pH=7. However, the K_d of AT1.03 increases with temperature. Taken together, its properties make AT1.03 well suited to monitor intracellular ATP concentrations at temperature-controlled conditions.

Using a CFP-YFP fusion protein linked by a protease recognition sequence, evidence was provided that FRET from CFP to YFP can be directly affected by [ATP] between 1–10 mM (34). However, this fusion protein does not contain any consensus ATP-binding motifs. In a follow-up study, it was demonstrated that ATP interacts with CFP via a histidine residue at position 148 (35). Although the CFP component of ATeam possesses this residue, changes in ATP concentration between 0–10 mM did not affect the FRET signal of an ATeam mutant lacking the ε subunit ATP-binding motif (25). This demonstrates that ATP does not directly affect the ATeam FRET pair (*i.e.* independent of ε subunit binding).

In comparison with traditional methods applying firefly luciferase, a potential disadvantage of the AT1.03 biosensor is its sensitivity over a relatively small range of ATP concentrations. To address this issue, a series of ATeam variants were generated displaying different ATP affinities. Substitution of the *B. subtilis* ε subunit with homologous subunits or mutated ε subunits carrying mutations within the interface between the N- and C-terminal domains altered ATP binding affinity without affecting ATP specificity (25). Several ATeam variants have been engineered (Table 1). AT3.10, a high-affinity variant (K_d= 7.4 μM) contains the ε subunit from the thermophilic *Bacillus* sp. PS3. In addition, $AT3.10^{MGK}$ (K_d=14 μM) and $AT1.03^{YEMK}$ (K_d=1.2 mM) were developed from AT3.10 and AT1.03, respectively, by mutating several residues in the domain interface.

Additionally a "negative control" ATeam unable to bind ATP was developed ($AT1.03^{R122K/R126K}$), in which two arginine residues essential for ATP binding were substituted by lysines.

ATeam sensors contain several optimizations to increase their dynamic range and SNR (*i.e.* they contain improved donor and acceptor fluorescent proteins). Wild-type GFP from *Aequoria victoria* is a weak dimer (*i.e.* it dimerizes only at high concentrations). To prevent artifacts in live cell studies, GFP, CFP, and YFP variants carrying the A206K mutation, which prevents dimerization (36), are generally applied. Also, the original AT1.03 biosensor contains the monomer-associated A206K mutation. To further increase ATeam's FRET efficiency, fluorescent proteins displaying a weak tendency for dimerization were developed. In this sense, AT1.03 containing the native K206A variant (AT1.03(nD/nA)) displayed an 28% increase in dynamic range (37).

Due to the wide spectral range of CFP and YFP, it is difficult to combine live cell imaging of CFP/YFP-based FRET biosensors with other fluorescent reporter molecules. However, a novel variant of ATeam (GO-ATeam) combines variants of GFP and an orange fluorescent protein (OFP) as a FRET pair (38). GO-ATeam can be combined with other UV-excitable fluorescent biosensors such as fura-2, a "classical" chemical sensor of free cytosolic calcium (Ca^{2+}) concentration (39).

Application of FRET-Based ATP Sensors

In contrast to classical bulk-phase total ATP measurements, fluorescence imaging of free [ATP] provides information about its cellular distribution and dynamics. Spatiotemporal imaging of human skin fibroblasts expressing AT1.03 suggests the presence of time-dependent [ATP] gradients in the cell processes (Fig. 2a–b). These local increases in [ATP] might serve to fuel the formation of actin filaments. Quantitative image analysis revealed that cell size increases over time (Fig. 2c) and that this increase was accompanied by a 20% decrease in average cellular AT1.03 FRET signal, followed by a 30% increase. (Fig. 2d–e). Studying the cellular compartmentalization of ATP-generating and -consuming systems (Fig. 1), as well as ATP transport, requires ATeams that are targeted to specific cellular locations. By attaching a triple repeat of the SV40 nuclear localization signal, ATeams can be expressed in the nuclear compartment. Similarly, ATeams can be targeted to the mitochondrial matrix using a tandem repeat of the mitochondrial targeting signal from cytochrome-*c* oxidase subunit VIII (cox8). Applying the above strategy, targeted ATeams have been used to examine the steady-state free ATP concentration in the cytosol, nucleus, and mitochondria in a HeLa cancer cell line (25). The FRET signal from cytosolic or nucleus-targeted ATeam was significantly higher than that of mitochondria-targeted ATeam, indicating that the free [ATP] is lower in the mitochondria of HeLa cells. The mitochondrial [ATP] is mainly determined by the rate of ATP synthesis by the F_oF_1-ATP synthase and ATP/ADP antiport by ANT. This means that a reduced ATP synthesis and/or rapid ATP/ADP exchange might be responsible for the lower mitochondrial [ATP]. It is currently unclear how much ATP is present in other cellular compartments like the ER, Golgi, and lysosomes. AT1.03 cannot be used to measure [ATP] in these compartments because it is glycosylated when targeted to these organelles. Moreover, the latter possess an acidic luminal pH that likely interferes with the FRET signal.

Analysis of the cellular metabolic state generally also requires information on the rate of ATP synthesis and hydrolysis rather than just steady-state free [ATP]. In this sense, quantifying the ATeam in response to metabolic perturbations can be used to obtain information about cell metabolism. For instance, the AT1.03 biosensor has been applied to measure the cytosolic free [ATP] in HeLa cells cultured in glucose and galactose medium (25). It was found that acute inhibition of the mitochondrial F_oF_1-ATP synthase using oligomycin rapidly decreased the cytosolic [ATP] in cells cultured in galactose medium. In contrast,

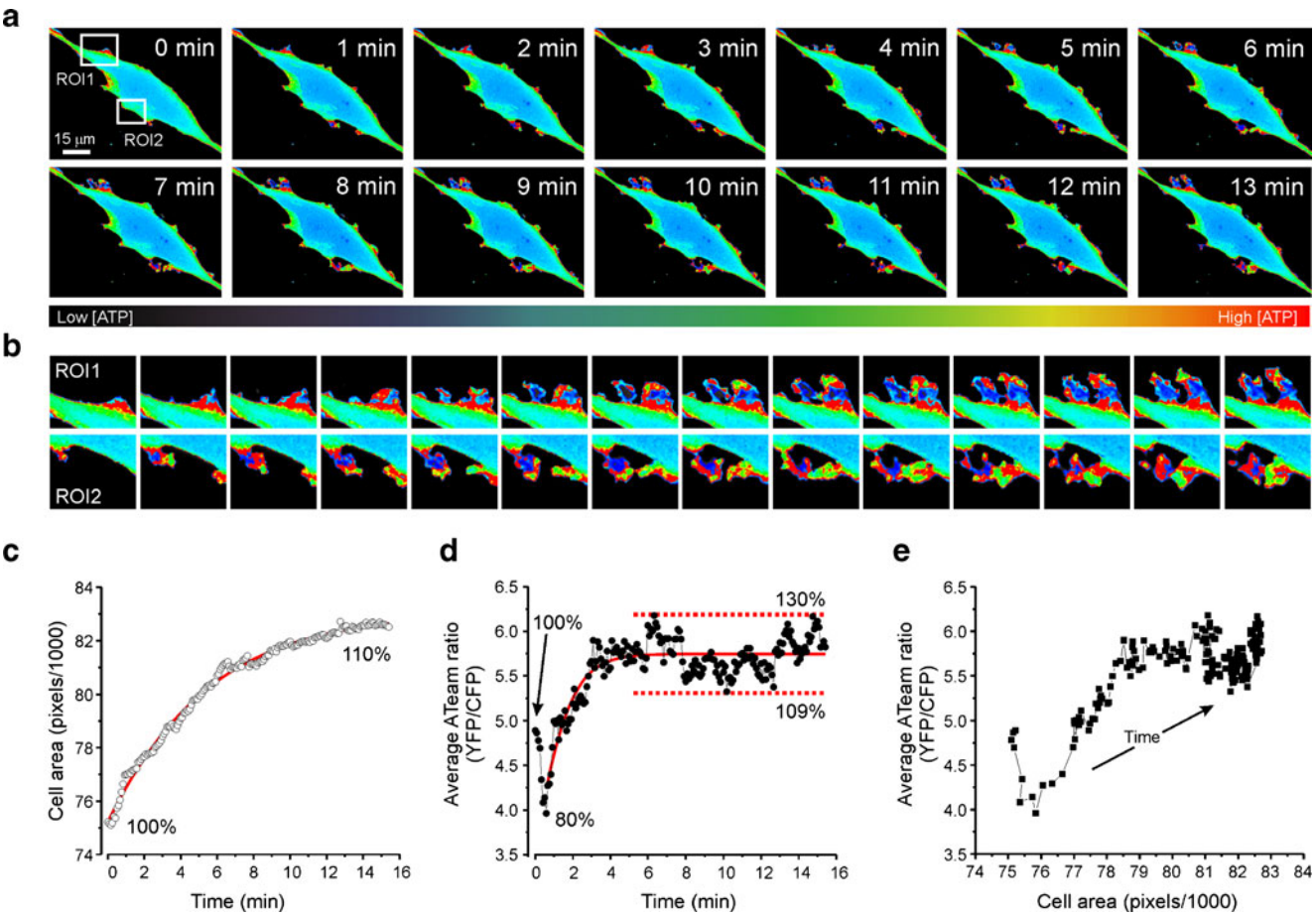

Fig. 2 Quantification of free cytosolic [ATP] in human skin fibroblasts. Skin fibroblasts of a healthy individual (cell line #5120) were transfected with the cytosolic free [ATP] sensor ATeam (Table 1: AT1.03) using a baculoviral system and subjected to serum-starvation. (**a**) Time-lapse analysis (images were recorded at 5 s time intervals; every 12th image is shown) of the cytosolic free [ATP], as reported by the ATeam YFP/CFP emission ratio. Fluorescence images were taken using a video-microscopy system [e.g. (42)]. Upon serum addition, local dynamic changes in [ATP] (cell protrusions) were observed, as exemplified by two regions of interest (ROI1, ROI2). (**b**) Magnification of the two ROIs in panel A. (**c**) Total cellular area quantified at full time resolution (5 s interval) for the image series in panel A. The continuous line represents a Boltzmann fit to the data ($R^2 = 0.99$, maximum = 83036 ± 99 (standard error) pixels). (**d**) Average cellular ATeam YFP/CFP emission ratio as a function of time. Percentages indicate the value of the ATeam emission ratio relative to the value at the start of the recording. The continuous line represents a Boltzmann fit to the data ($R^2 = 0.75$, maximum = 5.75 ± 0.02 (standard error) ratio value). (**e**) Relationship between cell area (x-axis, in pixels) and average cellular ATeam YFP/CFP emission ratio (y-axis).

oligomycin had no effect on cytosolic [ATP] in cells cultured in glucose medium. This result demonstrates that the type of sugar determines whether ATP is produced by glycolysis or OXPHOS.

Expression of mitochondria-targeted AT1.03 in human skin fibroblasts revealed an inhomogeneous ATeam ratio-signal (Fig. 3a). This suggests that individual mitochondria, as well as mitochondrial filaments that appear continuous, display an inhomogeneous free [ATP] distribution. When glucose in the extracellular medium was replaced by 2-DG, the ATeam CFP and YFP emission intensities increased and decreased, respectively, indicating a decrease in mitochondrial [ATP] (Fig. 3c). This demonstrates that an active glycolysis is crucial to maintain the mitochondrial [ATP] in human skin fibroblasts. Application of the mitochondrial protonophore FCCP (carbonyl cyanide-p-trifluoromethoxyphenylhydrazone), which depolarizes the mitochondrial membrane potential, induced an additional small change in CFP and YFP signals. Calculating the ATeam YFP/CFP ratio revealed that the free mitochondrial [ATP] was reduced upon glycolysis inhibition (Fig. 2b) in a biphasic manner (Fig. 3d; phase I and phase II). FCCP application did not further accelerate the rate of decay (phase III), supporting the above conclusion that an active glycolysis is crucial to maintain mitochondrial free [ATP] under these conditions.

Combined application of GO-ATeam and fura-2 in HeLa cells revealed that cell stimulation with the hormone histamine simultaneously increased the cytosolic free [Ca^{2+}] and mitochondrial free [ATP] (38). Moreover, the increase in mitochondrial [ATP] always occurred following the increase in cytosolic [Ca^{2+}]. These results are compatible with the idea that Ca^{2+} stimulates mitochondrial ATP production (17).

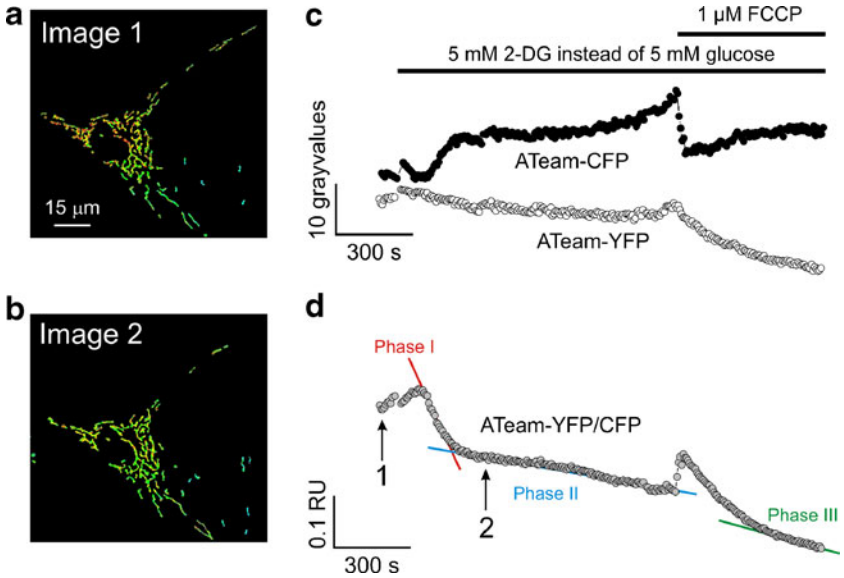

Fig. 3 Quantification of free mitochondrial [ATP] in human skin fibroblasts. Skin fibroblasts of a healthy individual (cell line #5120) were baculovirally transfected with a mitochondria-targeted (cox8) variant of the free [ATP] sensor ATeam (Table 1: AT1.03). Fluorescence images were taken using a video-microscopy system, and a mitochondrial mask was calculated as described previously (42). Cells were first placed in a medium with 5 mM glucose, next in a medium containing 5 mM of the glycolysis-inhibitor 2-Deoxy-D-glucose (2-DG) instead of glucose and, finally, treated with the mitochondrial protonophore FCCP (carbonyl cyanide-p-trifluoromethoxyphenylhydrazone). (**a**) Mitochondrial ATeam YFP/CFP ratio in untreated cells (image taken at time point marked by arrow 1 in panel D). (**b**) Mitochondrial ATeam YFP/CFP ratio in the presence of 2-DG instead of glucose (image taken at time point marked by arrow 2 in panel D). (**c**) YFP (open symbols) and CFP (filled symbols) fluorescence emission intensity of mitochondrial ATeam. (**d**) YFP/CFP ratio of mitochondrial ATeam. A fast (Phase I) and two slow phases (Phase II, III) are indicated.

CALIBRATION AND PITFALLS OF FRET-BASED GLUCOSE AND ATP SENSORS

Calibration

Using FRET-based sensors, alterations in [glucose] and [ATP] are reflected by changes in emission ratio between the respective fluorophores. In general, this approach allows comparison of glucose and ATP levels within the same cell (type) between individual experiments if the fluorescence recordings have been carried out under standardized conditions (*e.g.* temperature, excitation source, fluorescence filters). However, a proper cell-biochemical understanding of glucose and ATP metabolism requires knowledge about absolute concentrations. This means that the measured ratio (changes) need(s) to be translated into exact concentrations by means of calibration.

In case of glucose sensors, a method has been described that makes use of the *in vitro* K_d of the sensor (for details see (9,18,29,31)). A point of concern with this approach is that the *in vitro* K_d does not necessarily equal the *in vivo* 'apparent' K_d due to effects of the cellular environment. Nevertheless, an estimate of the *in vivo* 'apparent' K_d of the sensor can be obtained by varying the external glucose concentration and plotting the ratio signal of the cytosolic sensor as a function of external [glucose]. However, this strategy does not provide information about the absolute intracellular glucose concentration.

A more general protocol can be used for calibration of both cytosolic glucose and ATP sensors. This strategy relies on controlled PM permeabilization, followed by clamping the cytosolic glucose/ATP concentration with different levels of external glucose/ATP. Typically, cells are permeabilized using a detergent like digitonin, which interacts with PM cholesterol, or the pore-forming bacterial toxin *Streptolysin* O (SLO). To prevent morphological cell changes, damage to intracellular compartments, and cell detachment, the optimal permeabilization conditions need to be experimentally established for each cell type. Key parameters to consider are cell density, detergent concentration, detergent incubation time, and temperature. During permeabilization, the ionic composition and pH of the extracellular medium should closely mimic the intracellular situation. Another point of concern is the possible loss of intracellular proteins, including the sensor itself from the cell. To prevent this from happening, permeabilization should be as mild as possible, and holes in the PM should prevent passage of molecules >5 kDa. The calibration of organelle-targeted FRET sensors is still problematic. In the case of mitochondria, one possible strategy might involve isolation of mitochondria from the cell, followed by calibration using appropriate media and a spectrofluorometer.

Pitfalls

To facilitate signal detection, the discussed FRET sensors are often expressed using a strong promoter. If expression levels are too high, the sensor might act as a buffer and thereby influence glucose and/or ATP homeostasis. Buffering effects become particularly important if a sensor with a low K_d is expressed at a high level to detect a substrate that is present at a low concentration. To check for buffering effects, the ratio of the sensor can be plotted as a function of its expression level for individual cells. If buffering is absent, there should be no correlation between these parameters.

Another potential problem associated with high expression levels and/or the exogenous nature of the sensor protein is its breakdown by proteolysis. This can be investigated by Western blotting of (native) gels using an FP-specific antibody or in-gel fluorescence analysis (40). We have applied an insect (baculoviral) transfection system, as well as stable cell lines, to allow (controlled) expression of the sensor at relatively low levels.

Obviously, it is crucial to use a sensor with a detection range matching the expected range of metabolite concentrations in the cellular compartment. To validate the obtained results, parallel experiments with low- and high-affinity sensors might be relevant, as well as determining the detection range of the sensor by *in situ* calibration.

To rule out a specific effects on the signal of the FRET sensor, the best option is to carry out parallel experiments in which a "control" sensor (unable to bind the substrate) is used (Table 1; CT). For the presented glucose and ATP sensors, genuine alterations in metabolite concentration will induce opposite changes in the CFP and YFP emission intensity. For instance, in the case of AT1.03, an increase in free [ATP] will be associated with a decrease and increase in the CFP and YFP emission signal, respectively. In contrast, a pH change will increase or decrease the CFP and YFP signals in the same direction.

SUMMARY AND FUTURE PERSPECTIVES

Glucose constitutes a main source for ATP production in most mammalian cells, either directly by glycolysis (*e.g.* in cancer cells) or through the combined action of glycolysis and oxidative phosphorylation (Fig. 1). In addition to their role as substrates, glucose and ATP also act as regulators of metabolic pathways, placing these metabolites at the centre of cell metabolism. Metabolic dysfunction occurs during normal human aging and a large variety of pathological conditions, including type II diabetes, muscular dystrophies, inherited metabolic disorders, Parkinson's disease, Alzheimer's disease, metabolic syndrome, certain forms of cancer, and ischemia-reperfusion injury. Development of rational treatment strategies for these metabolic diseases requires a comprehensive understanding of how metabolic homeostasis is maintained and how cells respond to alterations in metabolic homeostasis. This information is also crucial to understanding the consequences of metabolic dysfunction induced by off-target drug effects (41). Because cell metabolism is dynamic and highly compartmentalized, experimental strategies are required that allow visualization of glucose and ATP concentration in time and space. Here, we presented how quantitative live cell microscopy of FRET-based protein sensors can be used for this purpose. We expect that this technology will be of great value to understanding the cell biological mechanism and consequences of metabolic dysfunction in patient-derived cells. Moreover, obtaining quantitative and spatiotemporal data is essential for construction of realistic mathematical models of metabolism. The latter will allow a systems-level understanding of metabolism in healthy and diseased cells and can be used to guide development of specific intervention strategies.

ACKNOWLEDGMENTS & DISCLOSURES

This work was supported by an equipment grant of NWO (Netherlands Organization for Scientific Research, No: 911-02-008), the Dutch Ministry of Economic Affairs (Innovative Onderzoeks Projecten (IOP) Grant: #IGE05003), and the CSBR (Centres for Systems Biology Research) initiative from NWO (No: CSBR09/013V). We are grateful to Dr. J.J. Esseling & Mr. A. Klymov (Dept. of Biochemistry, NCMLS) for performing ATeam microscopy experiments. We apologize to those authors whose articles we were unable to cite because of space limitations.

REFERENCES

1. Thorens B, Mueckler M. Glucose transporters in the 21st century. Am J Physiol Endocrinol Metab. 2010;298:E141–5.
2. Bittner CX, Loaiza A, Ruminot I, Larenas V, Sotelo-Hitschfeld T, Gutiérrez R, Córdova A, Valdebenito1 R, Frommer WB, Barros LF. High resolution measurement of the glycolytic rate. Front Neuroenergetics. 2010;15(2). pii: 26.
3. Blodgett DM, De Zutter JK, Levine KB, Karim P, Carruthers A. Structural Basis of GLUT1 Inhibition by Cytoplasmic ATP. J Gen Physiol. 2007;130(2):157–68.
4. Klip A, Tsakiridis T, Marette A, Ortiz PA. Regulation of expression of glucose transporters by glucose: a review of studies *in vivo* and in cell cultures. FASEB J. 1994;8(1):43–53.
5. John SA, Ottolia M, Weiss JN, Ribalet B. Dynamic modulation of intracellular glucose imaged in single cells using a FRET-based glucose nanosensor. Pflugers Arch. 2008;456(2):307–22.
6. Vander Heiden MG, Cantley LC, Thompson CB. Understanding the Warburg effect: the metabolic requirements of cell proliferation. Science. 2009;324:1029–33.

7. Gouyon F, Caillaud L, Carriere V, Klein C, Dalet V, Citadelle D, *et al.* Simple-sugar meals target GLUT2 at enterocyte apical membranes to improve sugar absorption: a study in GLUT2-null mice. J Physiol. 2003;552(Pt 3):823–32.
8. Tobin V, Le Gall M, Fioramonti X, Stolarczyk E, Blazquez AG, Klein C, *et al.* Insulin internalizes GLUT2 in the enterocytes of healthy but not insulin-resistant mice. J Physiol. 2003;552(Pt 3):823–32.
9. Fehr M, Takanaga H, Ehrhardt DW, Frommer WB. Evidence for high-capacity bidirectional glucose transport across the endoplasmic reticulum membrane by genetically encoded fluorescence resonance energy transfer nanosensors. Mol Cell Biol. 2005;25 (24):11102–12.
10. Rencurel F, Waeber G, Antoine B, Rocchiccioli F, Maulard P, Girard J, *et al.* Requirement of glucose metabolism for regulation of glucose transporter type 2 (GLUT2) gene expression in liver. Biochem J. 1996;314(Pt 3):903–9.
11. Simpson IA, Dwyer D, Malide D, Moley KH, Travis A, Vannucci SJ. The facilitative glucose transporter GLUT3: 20 years of distinction. Am J Physiol Endocrinol Metab. 2008;295(2):E242–253.
12. Mohan S, Sheena A, Poulose N, Anilkumar G. Molecular dynamics simulation studies of GLUT4: substrate-free and substrate-induced dynamics and ATP-mediated glucose transport inhibition. PLoS One. 2010;5(12):e14217.
13. Robey RB, Hay N. Mitochondrial hexokinases: guardians of the mitochondria. Cell Cycle. 2005;4(5):654–8.
14. Cairns RA, Harris IS, Mak TW. Regulation of cancer cell metabolism. Nat Rev Cancer. 2011;11:85–95.
15. Koopman WJH, Nijtmans LG, Dieteren CEJ, Roestenberg P, Valsecchi F, Smeitink JAM, *et al.* Mammalian mitochondrial complex I: Biogenesis, regulation and reactive oxygen species generation. Antioxid Redox Signal. 2010;12:1431–70.
16. Kahn BB, Alquier T, Carling D, Hardie DG. AMP-activated protein kinase: ancient energy gauge provides clues to modern understanding of metabolism. Cell Metab. 2005;1(1):15–25.
17. Griffiths EJ, Rutter GA. Mitochondrial calcium as a key regulator of mitochondrial ATP production in mammalian cells. Biochim Biophys Acta. 2009;1787(11):1324–33.
18. Fehr M, Lalonde S, Lager I, Wolff MW, Frommer WB. *In vivo* imaging of the dynamics of glucose uptake in the cytosol of cos-7 cells by fluorescent nanosensors. J Biol Chem. 2003;278 (21):19127–33.
19. Tsuboi T, Lippiat JD, Ashcroft FM, Rutter GA. ATP-dependent interaction of the cytosolic domains of the inwardly rectifying K^+ channel Kir6.2 revealed by fluorescence resonance energy transfer. Proc Natl Acad Sci U S A. 2004;101(1):76–81.
20. Deuschle K, Okumoto S, Mehr F, Looger L, Kozhukh L, Frommer WB. Construction and optimization of a family of genetically encoded metabolite sensors by semirational protein engineering. Protein Sci. 2005;14(9):2304–14.
21. Deuschle K, Fehr M, Hilpert M, Lager I, Lalonde S, Looger LL, *et al.* Genetically encoded sensors for metabolites. Cytometry A. 2005;64(1):3–9.
22. Deuschle K, Chaudhuri B, Okumoto S, Lager I, Lalonde S, Frommer WB. Rapid metabolism of glucose detected with FRET glucose nanosensors in epidermal cells and intact roots of *Arabidopsis* RNA-silencing mutants. Plant Cell. 2006;18(9):2314–25.
23. Okumoto S, Takanaga H, Frommer WB. Quantitative imaging for discovery and assembly of the metabo-regulome. New Phytol. 2008;180(2):271–95.
24. Berg J, Hung YP, Yellen G. A genetically encoded fluorescent reporter of ATP:ADP ratio. Nat Methods. 2009;6(2):161–6.
25. Imamura H, Nhat KP, Togawa H, Saito K, Iino R, Kato-Yamada Y, *et al.* Visualization of ATP levels inside single living cells with fluorescence resonance energy transfer-based genetically encoded indicators. Proc Natl Acad Sci U S A. 2009;106 (37):15651–6.
26. Lakowicz JR. Principles of fluorescence spectroscopy, chapter 13. 3rd ed. New York: Springer; 2006. p. 445–6.
27. Nagai T, Yamada S, Tominaga T, Ichikawa M, Miyawaki A. Expanded dynamic range of fluorescent indicators for Ca(2+) by circularly permuted yellow fluorescent proteins. Proc Natl Acad Sci U S A. 2004;101(29):10554–9.
28. Griesbeck O, Baird GS, Campbell RE, Zacharias DA, Tsien RY. Reducing the environmental sensitivity of yellow fluorescent protein. Mechanism and applications. J Biol Chem. 2001;276 (31):29188–94.
29. Takanaga H, Chaudhuri B, Frommer WB. GLUT1 and GLUT9 as major contributors to glucose influx in HepG2 cells identified by a high sensitivity intramolecular FRET glucose sensor. Biochim Biophys Acta. 2008;1778(4):1091–9.
30. Nagai T, Ibata K, Park ES, Kubota M, Mikoshiba K, Miyawaki A. A variant of yellow fluorescent protein with fast and efficient maturation for cell-biological applications. Nat Biotechnol. 2002;20(1):87–90.
31. Takanaga H, Frommer WB. Facilitative plasma membrane transporters function during ER transit. FASEB J. 2010;24 (8):2849–58.
32. Nagai T, Sawano A, Park ES, Miyawaki A. Circularly permuted green fluorescent proteins engineered to sense Ca^{2+}. Proc Natl Acad Sci USA. 2001;98:3197–202.
33. Yagi H, Kajiwara N, Tanaka H, Tsukihara T, Kato-Yamada Y, Yoshida M, *et al.* Structures of the thermophilic F1-ATPase epsilon subunit suggesting ATP-regulated arm motion of its C-terminal domain in F1. Proc Natl Acad Sci USA. 2007;104 (27):11233–8.
34. Willemse M, Janssen E, de Lange F, Wieringa B, Fransen J. ATP and FRET—a cautionary note. Nat Biotechnol. 2007;25(2):170–2.
35. Borst JW, Willemse M, Slijkhuis R, van der Krogt G, Laptenok SP, Jalink K, *et al.* ATP changes the fluorescence lifetime of cyan fluorescent protein via an interaction with His148. PLoS One. 2010;5(11):e13862.
36. Zacharias DA, Violin JD, Newton AC, Tsien RY. Partitioning of lipid-modified monomeric GFPs into membrane microdomains of live cells. Science. 2002;296(5569):913–6.
37. Kotera I, Iwasaki T, Imamura H, Noji H, Nagai T. Reversible dimerization of Aequorea victoria fluorescent proteins increases the dynamic range of FRET-based indicators. ACS Chem Biol. 2010;5(2):215–22.
38. Nakano M, Imamura H, Nagai T, Noji H. Ca^{2+} regulation of mitochondrial ATP synthesis visualized at the single cell level. ACS Chem Biol. 2011 (in press).
39. Tsien RY, Rink TJ, Poenie M. Measurement of cytosolic free Ca^{2+} in individual small cells using fluorescence microscopy with dual excitation wavelengths. Cell Calcium. 1985;6(1–2):145–57.
40. Dieteren CEJ, Willems PHGM, Vogel RO, Swarts HG, Fransen J, Roepman R, *et al.* Subunits of mitochondrial complex I exist as part of matrix- and membrane-associated subcomplexes in living cells. J Biol Chem. 2008;283(50):34753–61.
41. Wallace KB. Mitochondrial off targets of drug therapy. Tr Pharm Sci. 2010;29:361–6.
42. Koopman WJH, Distelmaier F, Esseling JJ, Smeitink JAM, Willems PHGM. Computer-assisted live cell analysis of mitochondrial membrane potential, morphology and calcium handling. Methods. 2008;46:304–11.